Applied Physics Letters

RESEARCH ARTICLE | OCTOBER 17 2024

Experimental implementation of time reversal in an optical domain

Wenxiu Yao ; Li-ang Zheng; Xiaoli Zhang ; Long Tian ; Heng Shen ; Yaohui Zheng

Appl. Phys. Lett. 125, 164005 (2024)
https://doi.org/10.1063/5.0207332

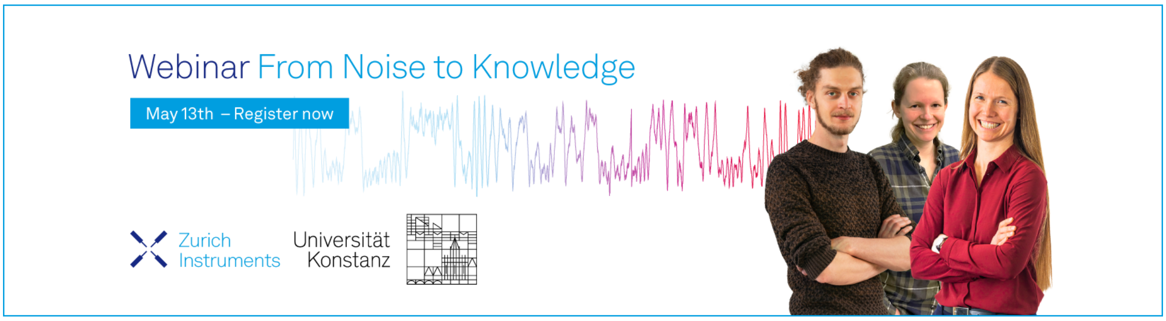

AIP Publishing

Applied Physics Letters ARTICLE pubs.aip.org/aip/apl

Experimental implementation of time reversal in an optical domain

Cite as: Appl. Phys. Lett. **125**, 164005 (2024); doi: 10.1063/5.0207332
Submitted: 7 March 2024 · Accepted: 8 October 2024 ·
Published Online: 17 October 2024

View Online Export Citation CrossMark

Wenxiu Yao,[1] Li-ang Zheng,[1] Xiaoli Zhang,[1] Long Tian,[1,2,a)] Heng Shen,[1,2,a)] and Yaohui Zheng[1,2,a)]

AFFILIATIONS

[1]State Key Laboratory of Quantum Optics and Quantum Optics Devices, Institute of Opto-Electronics, Shanxi University, Taiyuan 030006, China
[2]Collaborative Innovation Center of Extreme Optics, Shanxi University, Taiyuan 030006, China

[a)]Authors to whom correspondence should be addressed: tianlong@sxu.edu.cn; hengshen@sxu.edu.cn; and yhzheng@sxu.edu.cn

ABSTRACT

Time reversal has enabled many fundamental breakthroughs through the exquisite control over the complex systems. More recently, time reversal is predicted to be capable of enhancing the quantum sensing in unprecedented ways. Here, we report the experimental demonstration of time reversal based on a unitary and orthogonal squeezing interaction in an optical domain. Two cascaded degenerate optical parametric amplifiers are used to judiciously achieve a time reversal protocol. Finally, the concept of high-fidelity time reversal is demonstrated in the optical domain, offering remarkable opportunities for investigating many-body simulation and achieving quantum-enhanced sensing.

Time reversal has emerged as a powerful tool to understand complex systems since Loschmidt took into account time-reversing an entropy-increasing collision.[1] The high degree of controllability in the dynamics of quantum systems has enabled time reversal to play an essential role in historically disparate fields of physics. While Hahn spin echoes[2] in nuclear magnetic resonance spectroscopy employs time reversal of non-interacting quantum systems, recent progress in measuring out-of-time-ordered correlation to evaluate the quantum information scrambling, quantum many-body problems, and quantum system evolution is attained by implementing many-body time reversal protocols.[3–6] By means of the forward and backward time-evolutions, the time reversal can filter out some uninteresting effects, while amplifying other, more important physical processes taking place in complex quantum systems. Moreover, time reversal based on squeezing operations is strikingly believed to be associated with quantum-enhanced sensing approaching the Heisenberg limit.[7–12]

Quantum-enhanced sensing utilizing the time reversal of squeezing interaction has been demonstrated in a variety of physical systems, including spin systems,[13,14] trapped-ion mechanical oscillator,[15] and circuit quantum electrodynamics,[16] as well as the photon based on the SU (1, 1) interferometer.[17–19] Our group demonstrated a quantum precise measurement with the signal-to-noise ratio (SNR) improvement of 1.87 times based on two degenerate optical parametric amplifiers (DOPAs) in the optical domain, overcoming the challenge of controlling the cavity length and phase and the influence of external loss during the measurement.[20] However, since the physical system is non-perfect, the SNR improvement is limited to a relatively low level. It is of utmost importance to effectively evaluate the performance of the squeezing interaction for the construction of a time reversal system.

The key idea of achieving time reversal of the squeezing interaction is: a unitary evolution from a classical state to a non-classical state, and then reversely evolving the non-classical state to the initial state by application of $-\hat{H}$.[21–24] The most critical stage in realizing time reversed dynamics is to make a sign flip of a Hamiltonian that is utilized to complete time-forward evolution come true. Experimentally, the process is driven by controlled phase imprinting. However, a non-perfection of the system will inevitably induce that the evolution state deviates from the vicinity of the initial state. Taking the time reversal in the optical domain, for example, the non-perfection mainly comes from the optical loss of the time reversal system and the phase noise of optical phase locking loops. Optical loss degrades the unitarity of the time reversal by replacing the lost correlated photons with a vacuum field. Phase noise affects the orthogonality of the reversal process owing to the noise coupling with the orthogonal quadrature. Therefore, we can evaluate the quality of the time reversal in virtue of the unitarity and orthogonality of time reversal.

Here, we report on an experimental proof of the principle of time reversal based on a unitary and orthogonal squeezing interaction in the optical domain. As an essential prerequisite to such a scenario, two cascaded DOPAs are employed to accomplish the squeezing interaction, a Hamiltonian $\hat{H}$ by the employment of the first DOPA to generate a non-classical state, reversely Hamiltonian $-\hat{H}$, exploiting the second DOPA. The second DOPA with flip pump phase drives the system back to the vicinity of the initial state. Importantly, attributed to technical improvements in phase noise and system loss to reduce the degradation from decoherence, near unitarity is promised with the fidelity of approximately 0.9 in a relatively large range of squeezing strength. This offers insights into the potential applications in quantum imaging and gravitational wave detection. In addition, the interaction of the DOPA process is similar to the all-to-all interaction in the Lipkin–Meshkov–Glick model, which can be used as a simplified model for understanding bosonic many-body systems, particularly in the study of collective variables and quantum phase transitions. In combination with homodyne and tomography, it offers the opportunities to explore the bosonic many-body simulation in the optical domain inaccessible with the platform of optical discrete variable system with a single photon. Our system can be used for studying quantum phase transitions and collective variables, such as magnetism.

For degenerate parametric downconversion, the Hamiltonian describing degenerate second order nonlinear processes $\hat{H}$ is[25]

$$\hat{H} = \hbar\omega_1 \hat{a}^\dagger \hat{a} + \hbar\omega_2 \hat{b}^\dagger \hat{b} + i\hbar\Lambda(\hat{a}^{\dagger 2}\hat{b} - \hat{a}^2\hat{b}^\dagger)/2, \tag{1}$$

where ω_1 and ω_2 are the frequencies of the signal (1064 nm) and pump (532 nm) fields, and the operators $\hat{a}$ and $\hat{b}$ are the annihilation operators of the signal and pump fields, respectively. The object Λ is the nonlinear coupling parameter. Applying this Hamiltonian $\hat{H}$ for duration t implements the squeezing process. According to the Hamiltonian $\hat{H}$ and the *Langevin equations*,[26] the amplitude and phase quadrature variances at the output of the singly resonant DOPA on resonance can be given by[27,28]

$$\hat{X}^{\pm}_{out} = \frac{4\gamma_{oc1}\left(\dfrac{\Lambda^2}{\gamma_2}\alpha_1^2\hat{X}^{\pm}_{ic2} + \gamma_{ic1}\hat{X}^{\pm}_{ic1} + \gamma_{l1}\right)}{4\Omega^2 + (\gamma_1 + \gamma_\pm)^2} + \frac{((2\gamma_{oc1} - \gamma_1 - \gamma_\pm)^2 + 4\Omega^2)\hat{X}^{\pm}_{oc1}}{4\Omega^2 + (\gamma_1 + \gamma_\pm)^2}, \tag{2}$$

where the superscript "±" represents the amplitude and phase quadrature, respectively. The subscripts "*ic*" "*oc*," and "*l*" label terms relating to the input coupler, output coupler, and loss, respectively. The subscripts "1" and "2" denote the signal beam and pump beam. $\Omega = 12$ MHz is the Fourier frequency; $\alpha_1 = \sqrt{P_1/\hbar\omega_1}$ is the expectation value of the operation $\hat{a}$ that is the function of the signal power P_1; and $\gamma_{1,2} = \gamma_{ic1,2} + \gamma_{oc1,2} + \gamma_{l1,2}$ is the overall resonator decay rate; $\gamma_\pm$ is defined as

$$\gamma_\pm = \frac{\Lambda^2}{\gamma_2}\alpha_1^2 \pm \left(\frac{\Lambda^2}{2\gamma_2}\alpha_1^2 + \sqrt{\frac{2\Lambda^2}{\gamma_2}}\alpha_2\cos\theta\right), \tag{3}$$

where θ is the relative phase between the pump field and the signal field, i.e., twice the squeezed angle $\phi = \theta/2$. $\alpha_2 = \sqrt{P_2/\hbar\omega_2}$ is the expectation value of the operation $\hat{b}$ that is the function of the pump power P_2.

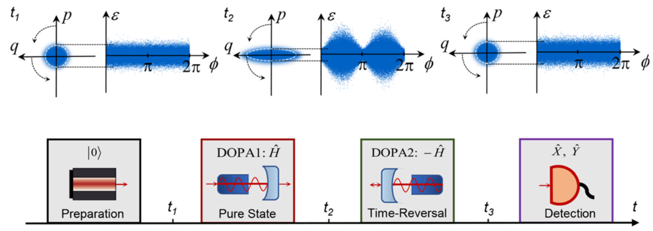

FIG. 1. Schematic diagram of time reversal of squeezing interaction is shown in the lower panel, while the upper panel shows phase spaces and electric field oscillations of light at different times. Squeezed state of light in $\hat{p}$-quadrature is generated by a degenerate optical parametric amplifier (DOPA1) pumped by a continuous-wave single-frequency laser. Then, the squeezed state into the DOPA2, where the relative phase θ' (defined as twice the squeezing angle ϕ of DOPA2) between the pump and the squeezed beam is locked to 0° in order to operate the anti-squeezing operation $\hat{H}' = -\hat{H}$ in $\hat{p}$-quadrature. The output beam from DOPA2 is finally detected with a balanced homodyne detection, achieving the time reversal in the optical domain.

The squeezed light, generated by DOPA1 with the Hamiltonian $\hat{H}$, is subsequently injected into DOPA2 as the signal light via the output coupling mirror (Fig. 1), i.e., $\hat{X}^{\pm'}_{oc1} = \hat{X}^{\pm}_{out}$. For DOPA2, the Hamiltonian with $\hat{H}' = -\hat{H}$ can be achieved through changing the relative phase $\theta' = \theta - \pi$ in the experiment. The corresponding variance of its amplitude quadrature and phase quadrature of the final output light after the DOPA2 can be derived and written as

$$\hat{X}^{\pm'}_{\mathrm{out}} = \frac{4\gamma_{oc1}(\gamma_{ic1}\hat{X}^{\pm'}_{ic1} + \gamma_{l1}) + ((2\gamma'_{oc1} - \gamma_1 - \gamma'_\pm)^2 + 4\Omega^2)\hat{X}^{\pm}_{\mathrm{out}}}{4\Omega^2 + (\gamma_1 + \gamma'_\pm)^2}. \tag{4}$$

When a vacuum state is the input state, the fidelity of the final state is expressed as,[29]

$$F = \frac{2}{\sqrt{(1 + \hat{X}^{+'}_{\mathrm{out}})(1 + \hat{X}^{-'}_{\mathrm{out}})}}. \tag{5}$$

For an experimental demonstration of time reversal by a unitary and orthogonal squeezing interaction, the experimental setup is shown in Fig. 2. Each DOPA used in this work is a semi-monolithic cavity consisting of a concave mirror and a periodically poled $KTiOPO_4$ crystal with the dimensions of $1 \times 2 \times 10\,\mathrm{mm}^3$. One end face of the crystal with a radius of curvature of 12 mm is coated as high reflectivity for the signal beam and high transmission for the pump beam, and the other end face is coated as anti-reflectivity for both beams. The concave mirror with a radius of curvature of 30 mm has high reflectivity for pump beam and a transmissivity of 18% for a signal beam. A piezoelectric transducer (PZT) is bonded to the concave mirror, serving as the control component. Moreover, the phase modulated signal with the modulation frequency of 32.6 MHz, is imprinted on the signal beam to generate error signal for controlling loops of DOPA1 and DOPA2.

Two key requirements for implementing the protocol must be satisfied, unitarity and orthogonality of two squeezing interactions. Generally, the former deteriorates as a result of decoherence or linking to the thermal bath,[30,31] which appears as an optical propagation loss and phase noise in the optical domain. In this experiment, the

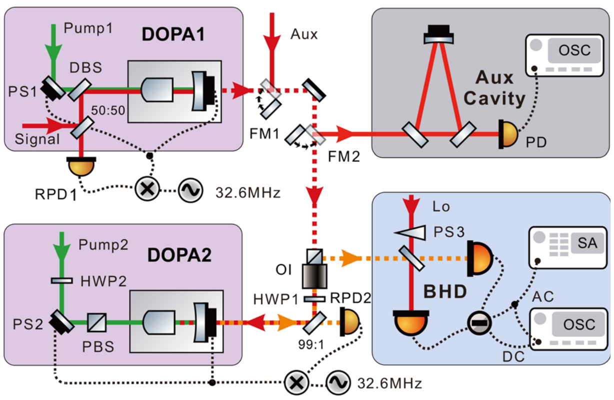

FIG. 2. Schematic diagram of the experimental setup. DOPA, degenerate optical parametric amplifier; Aux, auxiliary beam; Aux cavity, auxiliary ring cavity; PS, phase shifter; DBS, dichroic beam splitter; PZT, piezoelectric transducer; FM, flip mirror; HWP, half wave plate; PBS, polarization beam splitter; OI, optical isolator; PD, photodetector; RPD, resonant photodetector; BHD, balanced homodyne detection; Lo, local oscillator; SA, spectrum analyzer; and OSC, oscilloscope.

generated alternating current (AC) from resonant photodetector 1 (RPD1) or RPD2 is mixed with the phase modulated signal to yield an error signal, which is divided into two parts. One part is fed back to the PZT in the DOPA cavity to stabilize the DOPA cavity length on resonance, ensuring that the maximum squeezing degree is achieved. Afterward, by further technical improvement in system loss and phase noise, we manage the budget cautiously to guarantee the unitarity of squeezing interaction up to 8 dB. The other error signal is fed back to a phase shifter on the pump beam path to lock the relative phase θ between the pump field and the signal field. For DOPA1, θ is locked to 180°, which denotes that DOPA1 is operated at amplification (phase squeezed light). While for DOPA2, the relative phase θ' between the pump field and the injected signal field from DOPA1 is locked to 0°, thus the strict anti-squeezing interaction is performed on the signal field, which is exported from DOPA1. The output light from DOPA2 is separated from the injected signal beam by a half wave plate 1 (HWP1) and an optical isolator, it is then detected by a balanced homodyne detection (BHD) system.[32]

Actually, it is worth noting that the power of squeezed light exported from DOPA1 is in the order of few microwatts, which meets a lot of challenges in high-efficiency mode-matching of two DOPAs and accurate phase locking between the squeezed light from the DOPA1 and the pump light of the DOPA2. To address this issue of mode-matching, a bright auxiliary beam and flip mirrors are used, as shown in Fig. 2. By changing the angle of two flip mirrors, the auxiliary beam and squeezed light from the DOPA1 can enter the auxiliary ring cavity (finesses $\mathfrak{F} \approx 330$) in turn for mode matching. The output light of the auxiliary ring cavity is detected by a photodetector connected to an oscilloscope (OSC) to measure mode-matching efficiency. By implementing the high-efficiency mode-matching of the auxiliary ring cavity with both squeezed light and auxiliary beam, the same spatial mode of both beams is accurately ensured as well as the complete overlapping in space, and thus one can directly use such an auxiliary beam to accomplish the critical tasks aforementioned, which affect the final performance of our approach in terms of unitarity of two cascaded squeezing operations. In addition, by the employment of a self-developed electro-optic modulator[33,34] and a resonant photodetector with a high Q factor,[35,36] we achieve the ultra-low loss and drift-free servo loop, thereby ensuring the orthogonality between the two DOPAs.

As stated in the beginning, a unique feature of high-fidelity time reversal is obtained by squeezing operation $\hat{H}' = -\hat{H}$. It is determined by both the squeezing degree and the orthogonality of two squeezing operations. To observe this feature, we first vary the squeezing degree of DOPA2 by changing the pump power of DOPA2 (i.e., change the angle of HWP2) given the fixed squeezing level of DOPA1. In Fig. 3, experimental data in red dot with reduced value are in good agreement with theoretical prediction (red line). As shown in Fig. 3, with the squeezing degree of DOPA1 at (a) 3, (b) 4, (c) 6, and (d) 8 dB, respectively, the optimal fidelity appears when the squeezing degree of DOPA2 is close but lower than that of DOPA1. Here, the deviation is mainly due to the optical loss between two DOPAs, while the non-perfect unitary squeezing operations in DOPAs contribute a little. In addition, as we know, the higher the squeezing level, the more fragile the state is to dissipation. As a consequence, when raising the squeezing level further by injecting more pump light, the unitarity of squeezing interaction is more polluted, leading to the reduced fidelity in a higher squeezing level, as presented in Fig. 3. We should emphasize that the reduction of fidelity deterioration results from the dissipation in the whole implementation.

As mentioned before, orthogonality together with unitarity of two cascaded squeezing operation gives rise to the realization of time reversal with the optimal fidelity. To demonstrate the validity of such a statement, we vary the squeezing angle of DOPA2 relative to that of DOPA1 to characterize the process. Albeit it is challenging to actively lock the relative phase θ' of DOPA2 to arbitrary value, θ' can be passively stabilized during the measurement to record the time domain data. Experimentally, the direct-current (DC) output of the BHD is connected with a digital OSC to observe the interference signal of the output light and local oscillator. Then we employ the DC output of the BHD as the indicator of the squeezing angle of the DOPA2.

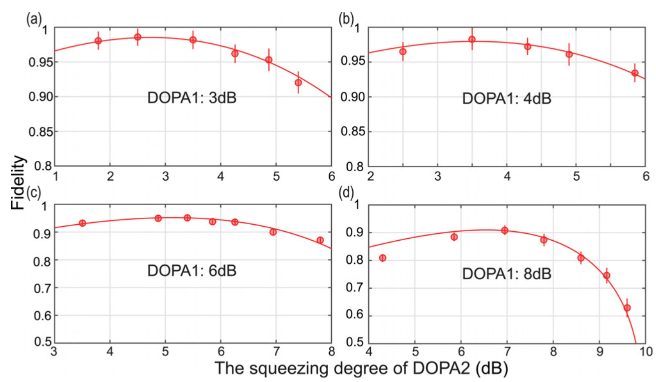

FIG. 3. Measured fidelity of the final state as a function of squeezing degree of DOPA2 for different squeezing level of DOPA1. The red solid line shows the theoretical values. The maximum fidelity can be achieved by accurately adjusting the performance of DOPA2 to satisfying the condition of $\hat{H}' = -\hat{H}$. Each data point is measured at the analysis frequency of 12 MHz. All data points denote averages over 30 experimental runs, and error bars are obtained by calculating the standard deviation of these results.

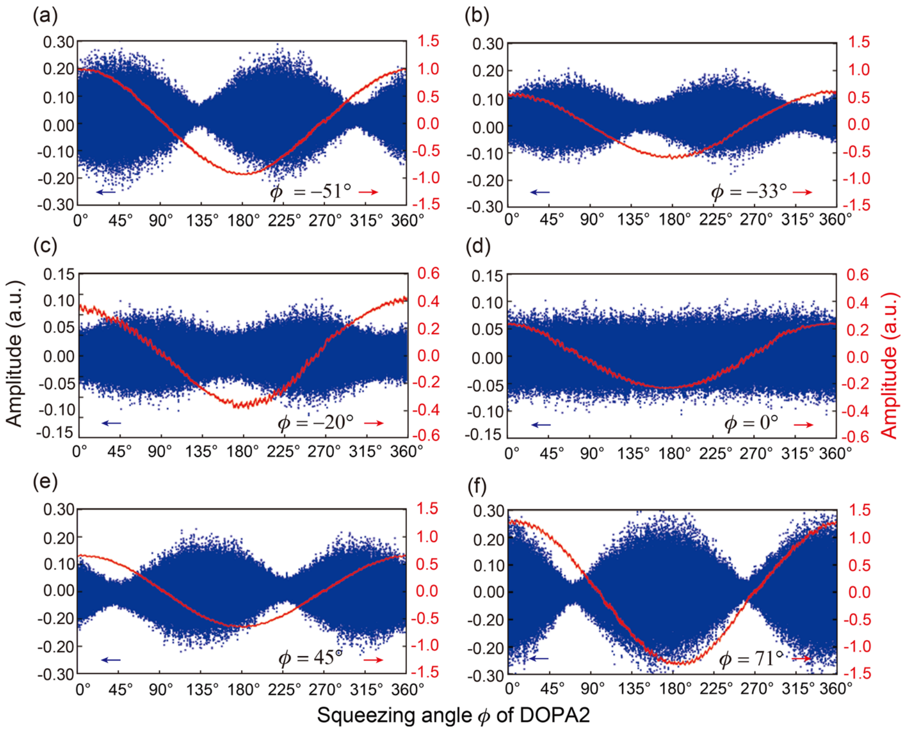

FIG. 4. Calibrating the squeezing angle of DOPA2 with respect to DOPA1 (8 dB). (a)–(f) illustrate the measured data with ϕ of (a) $-51°$, (b) $-33°$, (c) $-20°$, (d) $0°$, (e) $45°$, and (f) $71°$. At each ϕ, the panel shows the time domain quadrature values of quantum noise (blue dot), and the corresponding DC signal of the BHD (red curve).

In particular, the DC signal of BHD carrying the information of classical gain of DOPA2 is a function of the squeezing angle,

$$G_c(\theta') = \frac{1 + P_2'/P_{th} + 2\sqrt{P_2'/P_{th}}\cos\theta'}{(1 - P_2'/P_{th})^2}, \tag{6}$$

where P_2' is the pump power of DOPA2, $P_{th} = 390$ mW is the threshold power. With this formula, the corresponding values of θ' can be inferred.

The associated AC output is split by a power splitter with one half demodulated and amplified by a preamplifier at 12 MHz, then it is fed into an OSC to record the time domain signal of the final state[38] (Fig. 4). The other half is fed into a radio frequency spectrum analyzer to measure the noise level in the frequency domain, then the fidelity is calculated by the noise level (Fig. 5). Figure 4 showcases the demodulated AC and DC signals in time domain with ϕ of (a) $-51°$, (b) $-33°$, (c) $-20°$, (d) $0°$, (e) $45°$, and (f) $71°$. At each ϕ, the time domain-quadrature values (blue dot) and DC signal (red curve) are shown in Fig. 4. Finally, by reversing the squeezing interaction with DOPA2, the optical field returns to the vacuum state when $\phi = 0°$, as shown as Fig. 4(d). Figure 4 illustrates the associated noise distribution in the time domain, as expected by the formula in the text book.

To further characterize the orthogonality of our squeezing operations, we measure the noise level of the amplitude quadrature and phase quadrature components after squeezing and anti-squeezing, then the corresponding fidelity is calculated, as shown in Fig. 5. It is verified that the best fidelity can be achieved only under the condition of orthogonality between two cascaded squeezing, corresponding to the squeezing angle of DOPA2 ϕ of $0°$, the evaluation fidelity of 0.89 in Fig. 5.

We have provided an architecture of high-fidelity time reversal in the optical domain. Our experiment is carried out in two cascaded optical parametric amplifiers, wherein they are used to judiciously construct a time reversal device with two unitary and orthogonal squeezing operations. In particular, we provide a detailed account of the

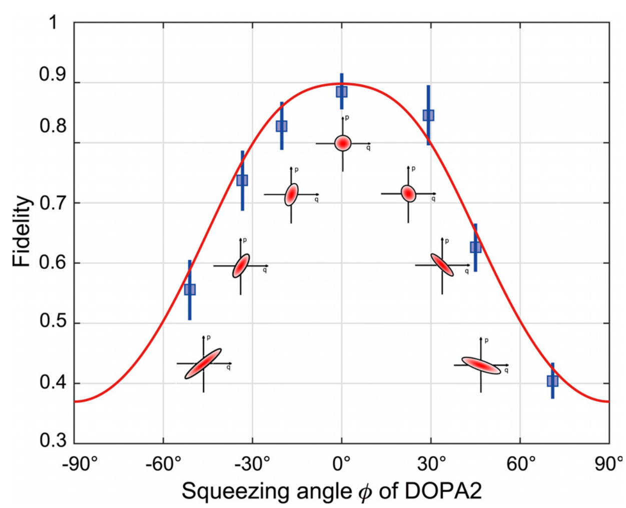

FIG. 5. Dependence of the fidelity on the squeezing angle ϕ of DOPA2. The fidelity is inferred at the squeezing strength of 8 dB. The inset shows reconstructed Wigner function distribution[37] obtained through the iterative maximum-likelihood estimation in phase space. Each data point is measured at 12 MHz. All data points denote averages over 30 experimental runs, and error bars are obtained by calculating the standard deviation of these results.

theory and quantitative explanation of the experimental results. Our results merge the rich physics of time reversal and their ability of high fidelity with the unique properties of time reversible interferometry. Owing to the technical improvements in optical phase locking loop and error signal extraction,[39] the fidelity of the time reversal state is approximately 0.9 at the squeezing strength of 8 dB. The demonstration offers the effective evaluation scheme for the performance of quantum-enhanced sensing system. Since the protocol is compatible with current LIGO[40,41] and VIRGO[42] detectors, this will provide basic evaluation technology for gravitational wave detection, as well as other quantum precision measurement systems. Moreover, the time reversal offers opportunities to explore the bosonic many-body simulation in an optical domain.

This work was supported by the National Natural Science Foundation of China (NSFC) (Grant Nos. 62225504, 62027821, 62035015, U22A6003, and 12174234) and the Fundamental Research Program of Shanxi Province (No. 202303021224006).

AUTHOR DECLARATIONS

Conflict of Interest

The authors have no conflicts to disclose.

Author Contributions

Wenxiu Yao: Data curation (lead); Investigation (lead); Writing – original draft (equal); Writing – review & editing (equal). **Li-ang Zheng:** Data curation (equal); Formal analysis (lead). **Xiaoli Zhang:** Data curation (equal); Investigation (equal). **Long Tian:** Conceptualization (equal); Validation (equal); Writing – original draft (equal); Writing – review & editing (equal). **Heng Shen:** Data curation (equal); Supervision (equal). **Yaohui Zheng:** Funding acquisition (equal); Methodology (equal); Project administration (equal); Resources (equal); Writing – review & editing (equal).

DATA AVAILABILITY

The data that support the findings of this study are available from the corresponding authors upon reasonable request.

REFERENCES

[1] J. Loschmidt, "Über den Zustand des Wärmegleichgewichtes eines Systems von Körpern mit Rücksicht auf die Schwerkraft," Sitzungsber. Kais. Akad. Wiss. Wien, Mathemat. Naturwiss. Classe, II. Abt. **73**, 128–142 (1876).
[2] E. L. Hahn, "Spin echoes," Phys. Rev. **80**, 580–594 (1950).
[3] M. Gärttner, J. G. Bohnet, A. Safavi-Naini, M. L. Wall, J. J. Bollinger, and A. M. Rey, "Measuring out-of-time-order correlations and multiple quantum spectra in a trapped-ion quantum magnet," Nat. Phys. **13**, 781–786 (2017).
[4] J. Li, R. Fan, H. Wang, B. Ye, B. Zeng, H. Zhai, X. Peng, and J. Du, "Measuring out-of-time-order correlators on a nuclear magnetic resonance quantum simulator," Phys. Rev. X **7**, 031011 (2017).
[5] B. Swingle, "Unscrambling the physics of out-of-time-order correlators," Nat. Phys. **14**, 988–990 (2018).
[6] S. Colombo, E. Pedrozo-Peñafiel, A. F. Adiyatullin, Z. Y. Li, E. Mendez, C. Shu, and V. Vuletić, "Time-reversal-based quantum metrology with many-body entangled states," Nat. Phys. **18**, 925–930 (2022).
[7] Z. Y. Ou, S. F. Pereira, and H. J. Kimble, "Quantum noise reduction in optical amplification," Phys. Rev. Lett. **70**, 3239 (1993).
[8] E. Davis, G. Bentsen, and M. Schleier-Smith, "Approaching the Heisenberg limit without single-particle detection," Phys. Rev. Lett. **116**, 053601 (2016).
[9] J. T. Jing, C. J. Liu, Z. F. Zhou, Z. Y. Ou, and W. P. Zhang, "Realization of a nonlinear interferometer with parametric amplifiers," Appl. Phys. Lett. **99**, 011110 (2011).
[10] E. Giese, S. Lemieux, M. Manceau, R. Fickler, and R. W. Boyd, "Phase sensitivity of gain-unbalanced nonlinear interferometers," Phys. Rev. A **96**, 053863 (2017).
[11] M. Manceau, G. Leuchs, F. Khalili, and M. Chekhova, "Detection loss tolerant supersensitive phase measurement with an SU(1,1) interferometer," Phys. Rev. Lett. **119**, 223604 (2017).
[12] Z. Y. Ou, "Enhancement of the phase-measurement sensitivity beyond the standard quantum limit by a nonlinear interferometer," Phys. Rev. A **85**, 023815 (2012).
[13] Q. Liu, L. N. Wu, J. H. Cao, T. W. Mao, X. W. Li, S. F. Guo, M. K. Tey, and L. You, "Nonlinear interferometry beyond classical limit enabled by cyclic dynamics," Nat. Phys. **18**, 167–171 (2022).
[14] D. Linnemann, H. Strobel, W. Muessel, J. Schulz, R. J. Lewis-Swan, K. V. Kheruntsyan, and M. K. Oberthaler, "Quantum-enhanced sensing based on time reversal of non-linear dynamics," Phys. Rev. Lett. **117**, 013001 (2016).
[15] S. C. Burd, R. Srinivas, J. J. Bollinger, A. C. Wilson, D. J. Wineland, D. Leibfried, D. H. Slichter, and D. T. C. Allcock, "Quantum amplification of mechanical oscillator motion," Science **364**, 1163–1165 (2019).
[16] M. Malnou, D. A. Palken, B. M. Brubaker, L. R. Vale, G. C. Hilton, and K. W. Lehnert, "Squeezed vacuum used to accelerate the search for a weak classical signal," Phys. Rev. X **9**, 021023 (2019).
[17] F. Hudelist, J. Kong, C. J. Liu, J. T. Jing, Z. Y. Ou, and W. P. Zhang, "Quantum metrology with parametric amplifier-based photon correlation interferometers," Nat. Commun. **5**, 3049 (2014).
[18] Z. Y. Ou and X. Y. Li, "Quantum SU(1,1) interferometers: Basic principles and applications," APL Photonics **5**, 080902 (2020).
[19] W. Du, J. Kong, G. Z. Bao, P. Y. Yang, J. Jia, S. Ming, C. H. Yuan, J. F. Chen, Z. Y. Ou, M. W. Mitchell, and W. P. Zhang, "SU(2)-in-SU(1,1) nested interferometer for high sensitivity, loss-tolerant quantum metrology," Phys. Rev. Lett. **128**, 033601 (2022).
[20] L. Tian, W. X. Yao, Y. M. Wu, Q. W. Wang, H. Shen, Y. H. Zheng, and K. C. Peng, "Loss-tolerant and quantum-enhanced interferometer by reversed squeezing processes," Opt. Lett. **48**, 3909–3912 (2023).
[21] C. M. Caves, "Quantum-mechanical noise in an interferometer," Phys. Rev. D **23**, 1693 (1981).
[22] B. Yurke, S. L. McCall, and J. R. Klauder, "SU(2) and SU(1,1) interferometers," Phys. Rev. A **33**, 4033 (1986).
[23] A. A. Clerk, M. H. Devoret, S. M. Girvin, F. Marquardt, and R. J. Schoelkopf, "Introduction to quantum noise measurement and amplification," Rev. Mod. Phys. **82**, 1155–1208 (2010).
[24] Y. Michael, L. Bello, M. Rosenbluh, and A. Peer, "Squeezing-enhanced Raman spectroscopy," npj Quantum Inf. **5**, 81 (2019).
[25] D. F. Walls and G. J. Milburn, *Quantum Optics* (Springer-Verlag, 1995).
[26] W. P. Bowen, "Experiments towards a quantum information network with squeezed light and entanglement," Ph.D. thesis (The Australian National University, 2003).
[27] K. McKenzie, N. Grosse, W. P. Bowen, S. E. Whitcomb, M. B. Gray, D. E. McClelland, and P. K. Lam, "Squeezing in the audio gravitational-wave detection band," Phys. Rev. Lett. **93**, 161105 (2004).
[28] X. C. Sun, Y. J. Wang, L. Tian, S. P. Shi, Y. H. Zheng, and K. C. Peng, "Dependence of the squeezing and anti-squeezing factors of bright squeezed light on the seed beam power and pump beam noise," Opt. Lett. **44**, 1789–1792 (2019).
[29] Q. W. Wang, Y. H. Tian, W. Li, L. Tian, Y. J. Wang, and Y. H. Zheng, "High-fidelity quantum teleportation toward cubic phase gates beyond the no-cloning limit," Phys. Rev. A **103**, 062421 (2021).
[30] E. Pedrozo-Peafiel, C. Shu, S. Colombo, A. F. Adiyatullin, Z. Y. Li, E. Mendez, B. Braverman, A. Kawasaki, D. Akamatsu, Y. H. Xiao, and V. Vuletic, "Entanglement on an optical atomic-clock transition," Nature **588**, 414–418 (2020).
[31] H. Bao, J. Duan, S. Jin *et al.*, "Spin squeezing of 10^{11} atoms by prediction and retrodiction measurements," Nature **581**, 159–163 (2020).
[32] J. R. Wang, Q. W. Wang, L. Tian, J. Su, and Y. H. Zheng, "A low-noise, high-SNR balanced homodyne detector for the bright squeezed state measurement in 1–100 kHz range," Chin. Phys. B **29**, 034205 (2020).

[33]S. P. Shi, L. Tian, Y. J. Wang, Y. H. Zheng, C. D. Xie, and K. C. Peng, "Demonstration of channel multiplexing quantum communication exploiting entangled sideband modes," Phys. Rev. Lett. **125**, 070502 (2020).
[34]Z. X. Li, W. G. Ma, W. H. Yang, Y. J. Wang, Y. H. Zheng, and K. C. Peng, "Reduction of zero baseline drift of the Pound–Drever–Hall error signal with a wedged electro-optical," Opt. Lett. **41**, 3331–3334 (2016).
[35]H. J. Zhou, W. H. Yang, Z. X. Li, X. F. Li, and Y. H. Zheng, "A bootstrapped, lownoise, and high-gain photodetector for shot noise measurement," Rev. Sci. Instrum. **85**, 013111 (2014).
[36]J. R. Wang, H. Y. Zhang, Z. L. Zhao, and Y. H. Zheng, "Realization of ultralow power phase locking by optimizing *Q* factor of resonant photodetector," Chin. Phys. B **29**, 124207 (2020).
[37]E. P. Wigner, "On the quantum correction for thermodynamic equilibrium," Phys. Rev. **40**, 749 (1932).
[38]G. Breitenbach, S. Schiller, and J. Mlynek, "Measurement of the quantum states of squeezed light," Nature **387**, 471 (1997).
[39]X. L. Jin, J. Su, Y. H. Zheng, C. Y. Chen, W. Z. Wang, and K. C. Peng, "Squeezed vacuum used to accelerate the search for a weak classical signal," Opt. Express **23**, 23859–23866 (2015).
[40]J. Aasi, J. Abadie, B. Abbott and *et al.*, "Enhanced sensitivity of the LIGO gravitational wave detector by using squeezed states of light," Nat. Photonics **7**, 613–619 (2013).
[41]M. Tse, H. C. Yu, N. Kijbunchoo *et al.*, "Quantum-enhanced advanced LIGO detectors in the era of gravitational-wave astronomy," Phys. Rev. Lett. **123**, 231107 (2019).
[42]F. Acernese, M. Agathos, K. Agatsuma, D. Aisa, N. Allemandou, A. Allocca, J. Amarni, P. Astone, G. Balestri, and G. Ballardin, "Advanced Virgo: A second-generation interferometric gravitational wave detector," Class. Quantum Grav. **32**, 024001 (2015).